Journal of Solid State Electrochemistry (2021) 25:1727–1741
https://doi.org/10.1007/s10008-021-04946-6

ORIGINAL PAPER

Structural, thermal, and ion dynamics studies of PVA-CS-NaI-based biopolymer electrolyte films

Devesh Chandra Bharati [1] · Pooja Rawat [1] · A. L. Saroj [1]

Received: 11 January 2021 / Revised: 24 March 2021 / Accepted: 25 March 2021 / Published online: 7 April 2021

Abstract

A series of biopolymer blend electrolytes (BPBEs) based on ((100-*x*)PVA-*x*CS)-NaI, viz. *BPBE-1* to *BPBE-5* (*x* = 10, 20, 30, 40, 50 in wt%), respectively, were prepared using solution cast technique. Prepared samples have been characterized using XRD, ATR-FTIR, TGA, and AC impedance spectroscopic techniques. ATR-FTIR results reveal the interactions between the constituents of PVA/CS with salt, NaI. XRD results show the semi-crystalline nature of PVA-CS polymer blend and %degree of crystallinity (X_c) was found to be minimum for sample *BPBE-1*. TGA and its 1st derivative (DTGA) results show that BPBE films decompose in multi-steps. The decomposition temperature peak ($T_{d,\ peak}$) associated with CS-PVA polymer blend and the interactions between CS-PVA-NaI have been discussed using TGA analysis. Temperature-dependent dc conductivity (σ_{dc}) and relaxation frequency (f_r) follow the Arrhenius type mechanism. The optimum $\sigma_{dc} \sim 1.2 \times 10^{-5}$ S/cm at 30 °C was received for sample, *BPBE-1*. The ac conductivity spectra for all samples follow the Jonscher's power law (JPL). Dielectric permittivity and electric modulus studies have also been done for understanding the charge storage properties and conductivity relaxation. Ionic transference number (ITN) measurement has been carried out for knowing the ionic/electronic nature of charge species. Cyclic voltammetry (CV) measurement has been done to study the electrochemical behavior of the optimized sample.

Keywords Biopolymer blend electrolytes · ATR-FTIR · TGA · XRD · Electrical properties · CV

Introduction

Solid polymer electrolytes (SPEs) based on biopolymers have emerged as promising materials due to their potential applications in electrochemical devices [1–3]. Biopolymer materials are non–toxic, naturally abundant, renewable, bio-degradable, cost-effective, and eco-friendly and can be easily obtained from natural sources like cell wall, plant, and animals [4–7]. Biopolymer/biodegradable polymer-based electrolytes have drawn much attention in recent years due to their eco-friendly nature and potential applications in electrochemical (EC) devices like super capacitors, dye-sensitized solar cells (DSSCs), and batteries [8–11]. The developments of polymer electrolyte based on biopolymer are of great interest due to presence of electron donor atoms such as O, N, etc. Donor atoms attached with the side chain of biopolymer interact weakly with the cations/anions of the dissociated salt present in the polymer electrolyte [1]. For the development of novel polymer electrolytes, biopolymers/or polysaccharides such as chitosan (CS), cellulose, and carboxymethyl cellulose (CMC) can be used as a host polymer network [12, 13]. Biopolymer, especially CS, has several advantages like good potential as host, abundant in nature, cheap, and eco-friendly, and it has β (1-4)-linked D-glucosamine de-acetylated linear polysaccharide [1, 6]. CS has two atoms O and N with lone pair electrons [1]. The hydroxyl (O–H), ether (C–O–C) group, and amine (NH_2) functional groups in the backbone of CS (as shown in Fig. 1) allow the possible interactions between the cations of salt as well as other polymers such as poly (vinyl alcohol), PVA, poly (vinyl pyrrolidone), PVP, etc. in terms of polymer blending [14]. The PVA has high population of O–H groups with its side chains, water soluble, and good dopant-dependent electrical and optical properties [14] which makes them suitable candidate for blending with the CS. A water-soluble nontoxic, biocompatible, biodegradable synthetic polymer, PVA can be used as host polymer for the preparation of polymer blend with biopolymer [15]. Due to presence of hydroxyl (O–H) group with the side chains of PVA backbone,

✉ A. L. Saroj
al.saroj@bhu.ac.in

[1] Department of physics, Institute of Science, BHU, Varanasi 221005, India

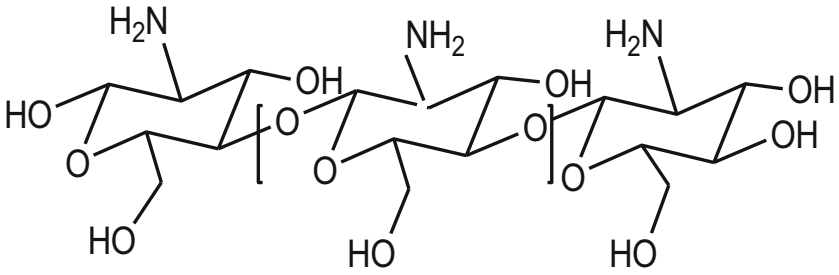

Fig. 1 Chemical structure and interacting sites (amine (NH_2) and hydroxyl (O–H)) of CS

this polymer interacts easily with the other polymers/biopolymers having some functional groups like CS and makes miscible polymer blend [16]. The use of single biopolymer may not be offered good mechanical flexibility and optical and chemical properties. Polymer blending is one of the promising approaches to enhance the ionic conductivity, mechanical flexibility, and optical properties of the electrolyte [17–19]. CS/PVA-ZnO-based nano-composite films reveal the antimicrobial activity [20]. Semi-crystalline phase of polymer network exhibits limited free space in between and along the polymer chains and there is restricted segmental motion of polymer chains. Whereas the amorphous phase of the network provides more free volume, mobility of charge carriers will be supported by segmental motion of polymer chains. The CS–PVA-based polymer blend film has very low ionic conductivity ~ 10^{-11} S cm^{-1} at room temperature [3]. In this work, the effect of CS↑/PVA↓ concentration on structural, thermal and ion transport properties of NaI-based biopolymer blend electrolyte (BPBE) films has been studied.

Experimental

Materials and sample preparation

PVA (M_w ~ 1.25 × 10^5 g/mol; purity > 98%), chitosan (M_w ~ 6 × 10^5 g/mol), and acetic acid (M_w ~ 60.05 g/mol) are purchased from Merck. The polymeric films based on ((100-*x*)PVA-*x*CS)-NaI, i.e., *BPBE-1* to *BPBE-5*, were prepared by varying the CS concentrations in wt% viz. 10, 20, 30, 40, 50, respectively. The solution casting method was used for the preparation of all samples. In this method, CS was first dissolved in 100-ml aqueous acetic acid solution (CS solution) and the solution containing suitable wt% of PVA and NaI was mixed with CS solution. The mixer having CS, PVA, NaI was stirred continuously with the help of a magnetic stirrer for 1 h at 60 °C until all these materials were dissolved completely and further continuous stirring for 48 h at same temperature for getting homogeneous viscous solution. Finally, this homogeneous viscous solution was poured on polypropylene Petri dishes (PDs) having diameter 10 cm, and solution-filled PDs were kept in the oven for few days at 40 °C to evaporate the solvent. The free standing flexible films having thicknesses ~ 90–100 μm were obtained and stored in evacuated silica gel-filled desiccators for further measurements.

Experimental procedure

Infrared (IR) spectroscopy was carried out for knowing the interactions between the functional groups of biopolymer/polymer with the additives like salt, NaI. The IR data in the wave number range 400–4000 cm^{-1} was taken by Perkin Elmer IR spectrometer (in attenuated total reflectance (ATR) mode) at the resolution of 1 cm^{-1}. X-ray diffraction (XRD) measurement was performed to determine the nature of the prepared film whether it is amorphous or crystalline using Philips X-ray diffractometer (PW 1710) having CuKα source with the wavelengths, λ = 1.5406 A° and 2θ from 5° to 70°. Thermo-gravimetric analysis (TGA) is an important tool to study the thermal stability of polymer electrolytes and the decomposition temperature of the constituents of the polymeric materials. The TGA measurement was performed using TGA/DSC-I (Mettler Toledo) at heating rate of 10 °C/min with temperature sensitivity ± 0.1 K. The impedance measurement was performed for prepared samples using HIOKI-3536 LCR meter in the frequency range 4 Hz to 8 MHz and the temperature range 30 to 90 °C with the interval of 10 °C.

Results and discussion

Fourier transform infrared analysis

Figure 2 shows the ATR-FTIR spectra of (a) CS, (b) PVA-CS, and (c–g) *BPBE-1 to BPBE-5*-based polymeric films, respectively. The CS-related band frequencies associated with N–H stretching, C–O stretching, amine (NH_2), carboxamide (O=C–NHR), and O–H stretching appeared at 890 cm^{-1}, 1022 cm^{-1}, 1548 cm^{-1}, 1641 cm^{-1}, and 3261 cm^{-1}, respectively [20]. The vibrational band frequencies of pure PVA appeared at 834 cm^{-1} (C–H rocking), 1249 cm^{-1} (C–C stretching), 1427 cm^{-1} (C–H bending) and 1723 cm^{-1} (C=O stretching) [16, 21]. It is expected that lone pair electrons of the nitrogen atom attached with CS backbone interact with C–O stretching of PVA and form a PVA-CS bio-polymer blend (Scheme 1). The complexation behavior is observed when Na^+ ion of the

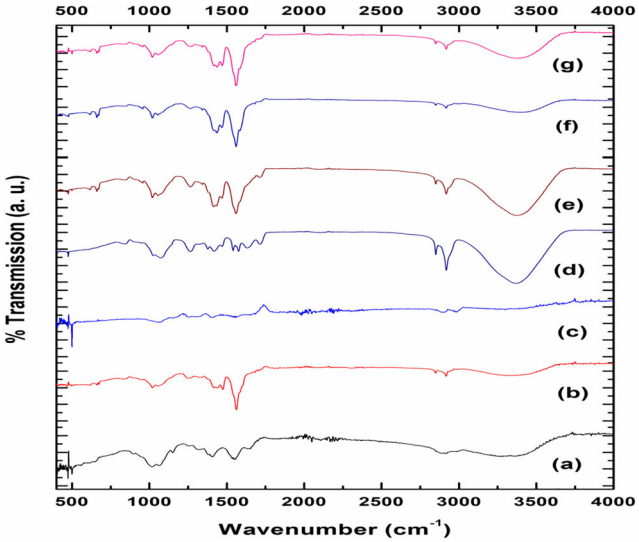

Fig. 2 ATR-FTIR spectra in the wavelength range 400–4000 cm^{-1} for **a** CS, **b** PVA-CS, **c**–**g** *BPBE-1* to *BPBE-5* with different composition of CS

dissociated salt, NaI interacts with functional groups of CS, i.e., amine (NH_2), carboxamide (O=C–NHR), and hydroxyl (O–H) group. Therefore, the vibration band frequencies associated with C–O stretching (1082 cm^{-1}), O–H stretching (3294 cm^{-1}) of pure PVA were found to shift at 1021 cm^{-1}, 1026 cm^{-1}, 1017 cm^{-1}, 1020 cm^{-1}, 1020 cm^{-1}, and 3370 cm^{-1}, 3373 cm^{-1}, 3392 cm^{-1}, 3369 cm^{-1}, 3371 cm^{-1} in bio-polymer blend *BPBE-1* to *BPBE-5*, respectively (Table 1). From Table 1, it is evident that the vibration band frequencies associated with CS also shifted/changed due to complexation with Na^+ ion of the dissociated salt. The above changes in the band frequencies associated with functional groups of PVA/CS clearly show the interaction/complexation with the dissociated salt, NaI (Table 1).

XRD analysis

The XRD patterns of prepared bio-polymer blend electrolytes are shown in Fig. 3. The PVA film has semi-crystalline in nature having characteristic peak centered at $2\theta = 19°$ with broad [15, 22]. The XRD pattern of CS shows that the characteristic peaks appeared at $2\theta = 10°$, 19°, and 22° with broad halos due to semi-crystalline nature of CS [21]. The characteristic peaks in XRD pattern associated with CS/PVA polymer blend were observed at $2\theta = 11°$, 19°, and 23° with broad halo (Fig. 3b). With the variation of CS content as 10, 20, 30, 40, 50 in ((100-*x*) PVA:*x*CS)/NaI-based BPBE films, the characteristic peaks of CS and PVA merged in to a single peak, centered at $2\theta = 23°$ (Fig. 3c–g) due to blending/cross-linking between the bio-polymer, CS, and polymer, PVA. The XRD patterns of CS/PVA/NaI-based BPBEs show that the halo portion of characteristic peak changes with the variation of CS concentration and 10 wt% CS containing sample has maximum amorphousness due to molecular interactions between the functional groups of CS and PVA. The addition of more CS enhanced the inter-molecular hydrogen bonding through the polymer blending between CS and PVA and thus results in formation of uniform arrangement of molecular chains and thus may develop the crystalline phase again in the polymer blend electrolyte system as shown in Fig. 3e–g. The % degree of crystallinity (X_c) has also been estimated from the XRD patterns using the relation:

Scheme 1 Possible interactions between the functional groups of polymer-biopolymer with dissociated salt

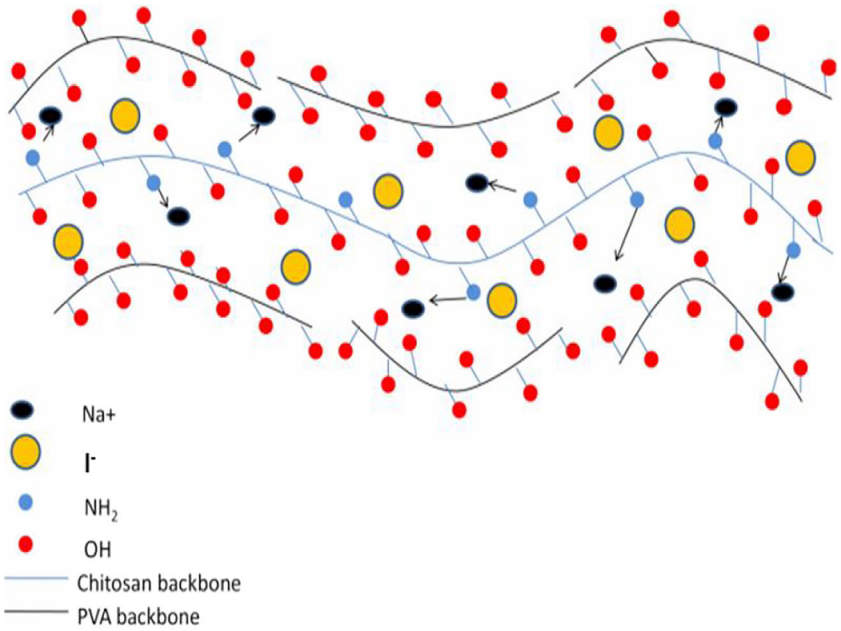

Table 1 Vibrational band assignments for the CS-PVA-NaI-based complexed bio-polymeric films

IR vibrational band frequencies (1 cm^{-1}) of ((100-*x*)PVA-*x*CS)-40NaI								
PVA [15, 16]	CS [20]	PVA-CS	*x* = 10	*x* = 20	*x* = 30	*x* = 40	*x* = 50	Band assignment
-	3371	-	-	3370	3374	3393	3397	NH_2-sym. stretching
3294	3261	-	3370	3373	3392	3369	3371	O–H stretching
2934	2896	2923	2899	2916	2917	2917	2922	C–H stretching
1723	1641	-	1664	1663	-	1680	1683	Amide (C=O)
-	1548	1565	1562	1576	1561	1560	1563	NH_2
1372	1243	1251	1255	1264	1262	1265	1269	CH waging
1082	1022	1022	1021	1026	1017	1020	1020	C–O stretching

$$X_c = \frac{S_c}{S_T} \times 100 \quad (1)$$

where S_c is the area under the crystalline peaks and S_T is the total area under the XRD patterns. The estimated X_c values are listed in Table 3. From Table 3, it is clear that the X_c value decreases/changes by varying the CS content in (100-*x*)PVA/*x*CS/40NaI. The reduction in crystallinity may be due to the interactions between the functional groups of CS-PVA as observed in ATR-FTIR spectra.

TGA analysis

TGA supported by 1st derivative of TGA (DTGA) thermograms of prepared BPBE films are shown in Fig. 4. The TGA and DTGA curves of CS-PVA and CS-PVA-NaI-based BPBE films show the multi-step decomposition (Fig. 4 f and a–e). From TGA curves, it is evident that there is weight loss ~ 10% between 40 and 110 °C due to the evaporation of moisture/solvent present in the prepared films [21]. The CS-based film decomposes in multi-steps that appeared at 281.3 °C and 363.4 °C associated with polysaccharide unit of CS [21] while PVA decomposes in multi-steps reported at 329.3 °C, 427.6 °C, and 449.3 °C [23]. From TGA thermograms (Fig. 4f), it is evident that CS-PVA-based blend decomposes in multi-steps that appeared at T_{d1} ~ 192.8 °C, T_{d2} ~ 288.9 °C, T_{d3} ~ 305.3 °C, and T_{d4} ~ 429.6 °C (Table 2) [20]. Due to the addition of NaI in CS-PVA, the decomposition peaks appeared at T_{d2} ~ 288.9 °C, and T_{d4} ~ 429.6 °C has found to shift at 232.5 °C and 410.9 °C, respectively, associated with decomposition of CS-PVA-NaI complexed. For the film containing 10 wt% CS, the decomposition peaks T_{d2}, T_{d3}, and T_{d4} were found to shift at 270.5 °C, 307.2 °C, and 425.7 °C, respectively. The above analysis clearly shows that due to variation of CS↑/PVA↓ ratio, the thermal stability enhanced due to cross linking between two polymers.

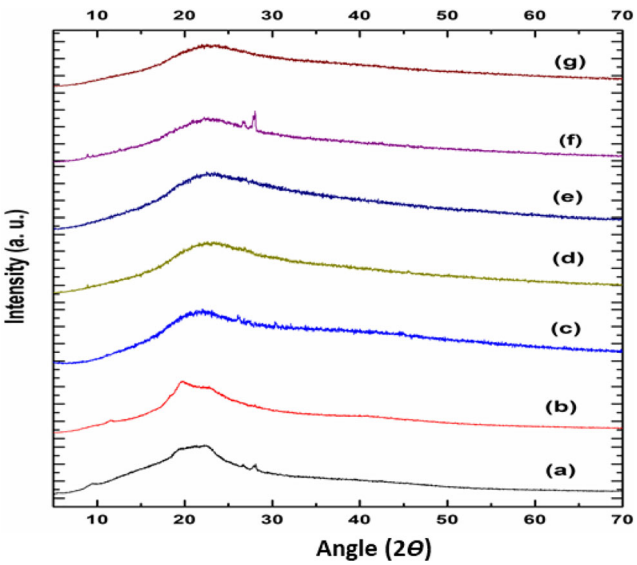

Fig. 3 XRD patterns of **a** CS, **b** PVA-CS, and **c**–**g** *BPBE-1* to *BPBE-5* biopolymeric systems with varying CS concentration

Impedance spectroscopic study

For the determination of impedance, i.e. $Z^*(\omega) = Z' + jZ''$ where Z' and Z'' are the real and imaginary parts of the impedance, the polymeric films having thickness in the range 0.04–0.06 cm were sandwiched in between stainless steel as blocking electrodes. The Cole-Cole plots for sample *BPBE-1* to *BPBE-5* at 30 °C and temperature-dependent Cole-Cole plots for sample *BPBE-1* at different temperatures are shown in Fig. 5a, b. These plots have well-defined two regions: (i) semi-circular region in high frequency associated with bulk resistance and slanted spike in low frequency region due to the blocking electrode/electrolyte interface, i.e., formation of double-

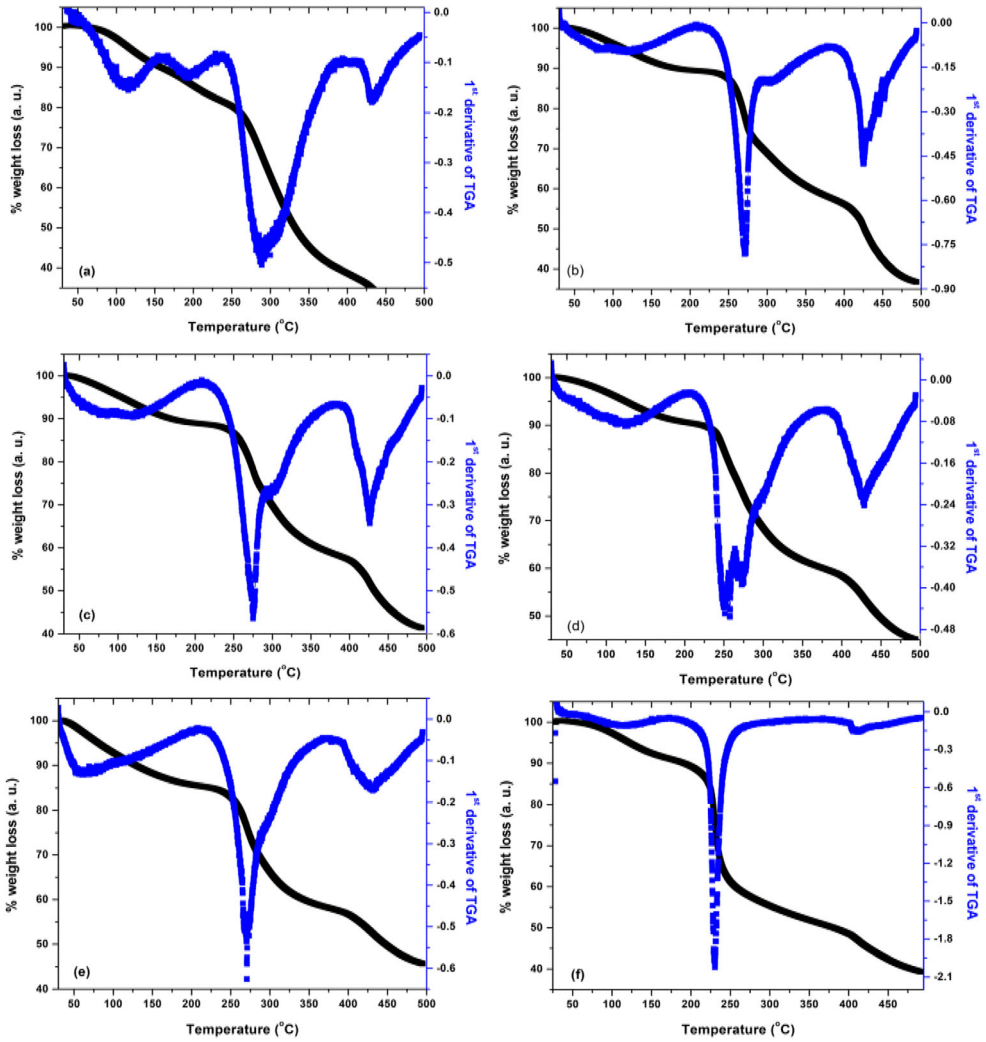

Fig. 4 TGA (supported by DTGA) thermograms of **a** CS-PVA and **b**–**f** *BPBE-1* to *BPBE-5*-based polymeric films having different CS content

layer capacitance. The bulk ionic conductivity of the sample has been calculated using the following relation:

$$\sigma_b = \frac{1}{R_b}\frac{t}{B} \tag{2}$$

where B is the contact area (cm^2) of the blocking electrode contact with sample, R_b is the bulk resistance, and t is the thickness (cm) of the film. The bulk ionic conductivity values for each prepared BPBE films are listed in Table 3. The sample, *BPBE-1*, shows optimum ionic conductivity ~ 1.2×10^{-5} S/cm at 30 °C. Therefore, the variation of CS content and

Table 2 Onset temperature ($T_{d,\ onset}$) and thermal decomposition temperature peaks ($T_{d,\ peaks}$) for CS-PVA-NaI-based BPBE films

Sample ((100-*x*)PVA:*x*CS):40NaI	Thermal decomposition temperature peaks ($T_{d,\ peak}$) (± .1) (°C) for CS-PVA-NaI-based BPBE films.				
	$T_{d,\ onset}$	$T_{d1,\ peak}$	$T_{d2,\ peak}$	$T_{d3,\ peak}$	$T_{d4,\ peak}$
PVA/CS	244.4	192.8	288.9	305.3	429.6
x = 10	232.6	118.0	270.5	307.2	425.7
x = 20	228.4	116.1	275.3	298.6	426.7
x = 30	221.7	121.1	251.2	273.4	426.7
x = 40	229.5	-	-	271.6	429.6
x = 50	207.6	-	232.5	-	410.9

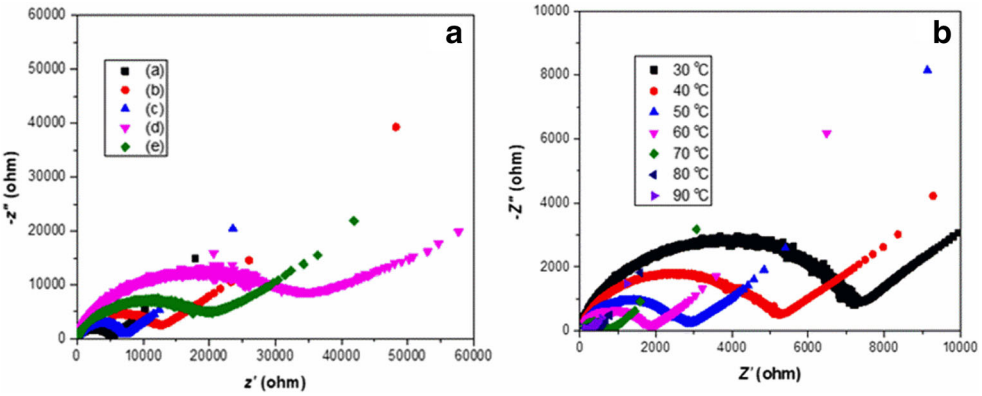

Fig. 5 Cole-Cole plots for **a** *BPBE-1* to *BPBE-5* with different composition of CS 30 °C and **b** *BPBE-1*-based film at different temperatures

incorporation of NaI have modified the ionic conductivity at 30 °C due to enhancement in the amorphous phase (reduction in the energy barrier of polymer chains) and availability of large number of free charge carriers. Temperature-dependent conductivity (log σ_b vs $1/T$) and dielectric relaxation frequency (log f_r vs $1/T$) plots for all prepared BPBE films are shown in Fig. 6. From Fig. 6a, it is observed that the conductivity for all samples increases with increasing temperature (obeys Arrhenius type behavior) in two regions above and below the glass transition temperature. The Arrhenius type temperature-dependent conductivity (σ_T) can be expressed as

$$\sigma_T = \sigma_b \exp\left[\frac{-E_a}{K_B T}\right] \quad (3)$$

whereσ_b, E_a, K_B, and T are the pre-exponential factor, activation energy, Boltzmann constant, and absolute temperature, respectively. Temperature affects the vibrational dynamics in the polymers, and hence, polymer chain relaxation resulted as change in availability of co-ordination sites and amorphousness within the host matrix. The log f_r vs $1/T$ plots (Fig. 6b) for prepared samples follows the same trend as observed in logσ_b vs $1/T$ plots and Arrhenius equation can be written as

$$f_T = f_b \exp\left[\frac{-E_a}{K_B T}\right] \quad (4)$$

Table 3 The values of conductivity (σ_b and σ_{dc}) and %degree of crystallinity (X_c)/amorphicity (1-X_c) for prepared BPBE films

Sample (100-x)PVA/xCS/NaI	1-χ_c	χ_c	σ_b (S/cm)	σ_{dc} (S/cm)
CS-PVA	.71	.29		
x = 10	.92	.09	1.20×10^{-5}	1.11×10^{-5}
x = 20	.92	.08	4.07×10^{-6}	5.01×10^{-6}
x = 30	.90	.10	9.61×10^{-6}	1.01×10^{-5}
x = 40	.88	.12	1.49×10^{-6}	2.20×10^{-6}
x = 50	.87	.13	2.05×10^{-6}	2.96×10^{-6}

where f_T is the temperature-dependent relaxation frequency, f_b is the constant, E_a (eV) is the activation energy, K_B is the Boltzmann constant, and T is the temperature in K. From Fig. 6, it has been observed that both the plots consist two regions, below glass transition (T_g) and above T_g, and the formations of local domains are possible due to cross-linking between two polymers, CS-PVA [24]. Below T_g, polymer blend matrix may be in frozen state attributed to the slow segmental motion of polymer chain. However, the polymer relaxation peaks were observed in prepared BPBE films and the occurrence of relaxation peaks and thereby conductivity are associated with motion of local segments of the network and ions hopping take place from one site to another site. Above the T_g, polymer network becomes rubbery and polymer chains are more flexible; hence, more free volume within the matrix is available [25, 26]. The E_a values below and above T_g are calculated from Fig. 6 and data are listed in Table 4. Below T_g, E_a values are quite small for all the samples (low activation energy is responsible for easier transportation of charge carries). Table 4 shows that E_a values (below and above T_g) obtained from log σ vs $1/T$ and log f_r vs $1/T$ plots are in good agreement.

AC conductivity study

Frequency-dependent conductivity spectra of the BPBEs films, prepared at x = 10, 20, 30, 40, 50 in the experimental frequency range (4 Hz to 8 MHz), are shown in the Fig. 7a. Similarly, Fig. 7b depicts the frequency-dependent conductivity spectra for the sample x = 10 at various temperatures. It is noticed that the frequency-dependent spectra of prepared films (either Fig. 7a or b) mainly consist of three regions namely the low-frequency dispersion region, mid-frequency plateau region, and high-frequency dispersion region. Low-frequency dispersive region is attributed to the fluctuations of the interfacial polarization at the electrode-sample interface. Low conductivity of the samples in this region is due to the presence of an opposing nature of internal electric field to

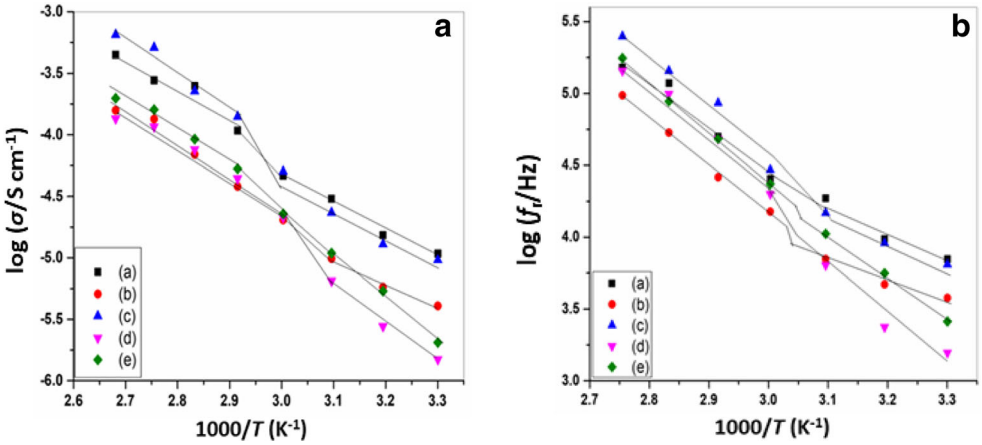

Fig. 6 Temperature dependence of **a** bulk conductivity and **b** dielectric relaxation frequency for samples *BPBE-1* to *BPBE-5* with different concentration of CS

the applied external electric field. The frequency-independent plateau regions on the curves in Fig. 7a correspond to bulk conductivity or dc conductivity (σ_{dc}). These plateau regions are shorten with CS content but elevate with increasing temperature (Fig. 7b) indicating increase in the dc conductivity. The third region, i.e., high-frequency dispersion region, appeared due to capacitive nature of the prepared films. Hence, the ac conductivity spectra of prepared biopolymer blend electrolyte films may be given by Jonscher's power law (JPL) [27, 28].

$$\sigma_f = \sigma_{dc} + Af^n \quad (5)$$

where n is the power law exponent, A the temperature-dependent parameter, σ_{dc} the dc conductivity, and f the frequency. The solid line in the ac conductivity spectra specifies the fit of experimental data to the JPL. The value of dc conductivity is following with the values calculated from Cole-Cole plot. The value of power law exponent, n, lies in the range of 0 to 1 for *BPBE* films.

Charge carrier concentration (N), ion diffusivity (D), and mobility (μ) study

The dc/bulk ionic conductivity is one of the important property of a solid polymer electrolyte which mostly depends on charge carrier concentration, N mobility, μ and can be expressed as $\sigma_{dc} = Ne\mu$, where e is the elementary charge. From this expression, mobility of charge carriers can be expressed as $\mu = \frac{\sigma_{dc}}{N e}$. From Fig. 11a, the values of tan δ_{peak} and f_{peak} were estimated for all samples (*BPBE-1* to *BPBE-5*) at 30 °C. The diffusion constant (or ion diffusivity), D, can be estimated by using the relation: $D = \frac{2\pi f_{peak} t^2}{32\left(\tan\delta_{peak}\right)}^3$ where t is the thickness of the sample, $\tan\delta_{peak}$ is the maximum value of loss tangent at peak frequency, f_{peak} [29]. Generally, μ depends upon three factors like size of ions, interaction between free ions with polymer chains and loan pair of electrons present in interactive groups of polymer [30]. The values of D, μ, and N have been calculated by using the above respective expressions and data are plotted as shown in Fig. 8. From Fig. 8, it has been observed that the sample *BPBE-1* having optimum dc conductivity has maximum N and μ value at 30 °C.

Table 4 Ionic transference number (ITN), power law exponent (n), activation energies (E_{a1}/E_{a2}), and diffusivity (D) values of BPBE films

BPBE films-(100-x)PVA/xCS/NaI	s	ITN	E_{a1}/E_{a2} (eV) from logσ vs. 1/T	E_{a1}/E_{a2} (eV) from logf_r vs. 1/T	D (cm^2/s)
x = 10	0.84	0.98	0.42/0.57	0.37/0.76	1.50×10^{-6}
x = 20	0.82	0.96	0.40/0.61	0.58/0.68	1.33×10^{-6}
x = 30	0.75	0.96	0.50/0.72	0.38/0.86	9.43×10^{-7}
x = 40	0.68	0.94	0.64/0.62	0.83/0.84	9.69×10^{-7}
x = 50	0.83	0.94	0.69/0.62	0.69/0.86	1.01×10^{-6}

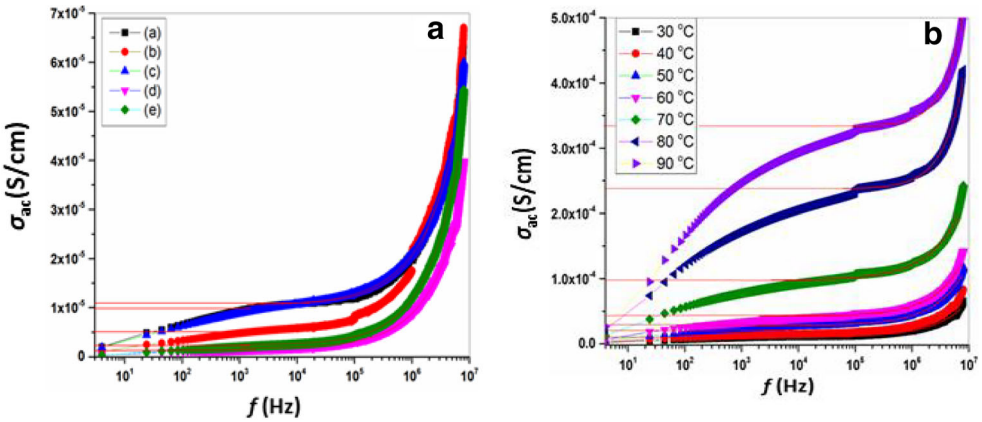

Fig. 7 AC conductivity spectra of **a** *BPBE-1* to *BPBE-5* with varying CS content and **b** for *BPBE -1* at different temperatures

Dielectric permittivity study

In ion conducting solid polymer electrolytes, the dielectric complex permittivity parameters (ε′ and ε″) have particular importance which show the ability of polymer to dissolve the salt and their energy storage capacity. The complex permittivity (ε*) relation can be expressed as

$$\varepsilon^*(\omega) = \varepsilon' - j\varepsilon'' = \frac{1}{J\omega c Z^*(\omega)} = \frac{Z''}{\omega C\left(Z'^2 + Z''^2\right)} - j\frac{Z'}{\omega C\left(Z'^2 + Z''^2\right)} \quad (6)$$

where ε' is the real part of the relative permittivity and ε'' is the imaginary part of the relative permittivity. The dielectric constant, ε', shows a dispersion from the low-frequency (static) permittivity, ε [$= \lim_{\omega\to 0}\varepsilon'(\omega)$], to the infinite frequency permittivity, ε_∞[$= \lim_{\omega\to\infty}\varepsilon''(\omega)$] expresses the energy dissipation. The real part of permittivity (ε') was estimated from the relation expressed as: $\varepsilon' = \frac{Ct}{\varepsilon_o B}$ where t is the thickness of the polymer film, B the area of the electrolyte films, C the capacitance, $\varepsilon_o = 8.854 \times 10^{-12}$ F m^{-1} (permittivity of free space). By using the relation $\varepsilon'' = \varepsilon' \tan\delta$, the dielectric loss, ε'' is calculated. The variations of dielectric constant (ε') and dielectric loss (ε'') for *BPBE-1* to *BPBE-5* at 30 °C and for *BPBE-1* at different temperatures are shown in Fig. 9 a, b and c, d, respectively. It is noted that ε' and ε'' for the electrolyte systems first decrease with increasing frequency and reached a constant value in high-frequency range (≥ 8 MHz). The high value of ε' and ε'' "at low frequency) are observed due to the accumulation of free charge carriers at the electrode-

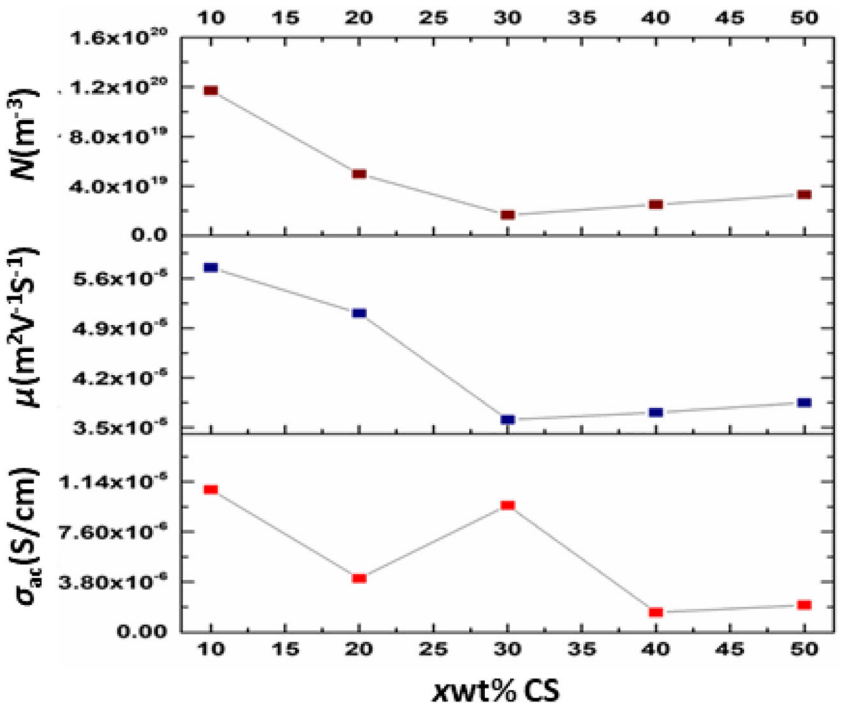

Fig. 8 Variation of dc conductivity (σ_{dc}), mobility (μ), and charge carrier concentration (N) as a function of concentration of CS at 30 °C

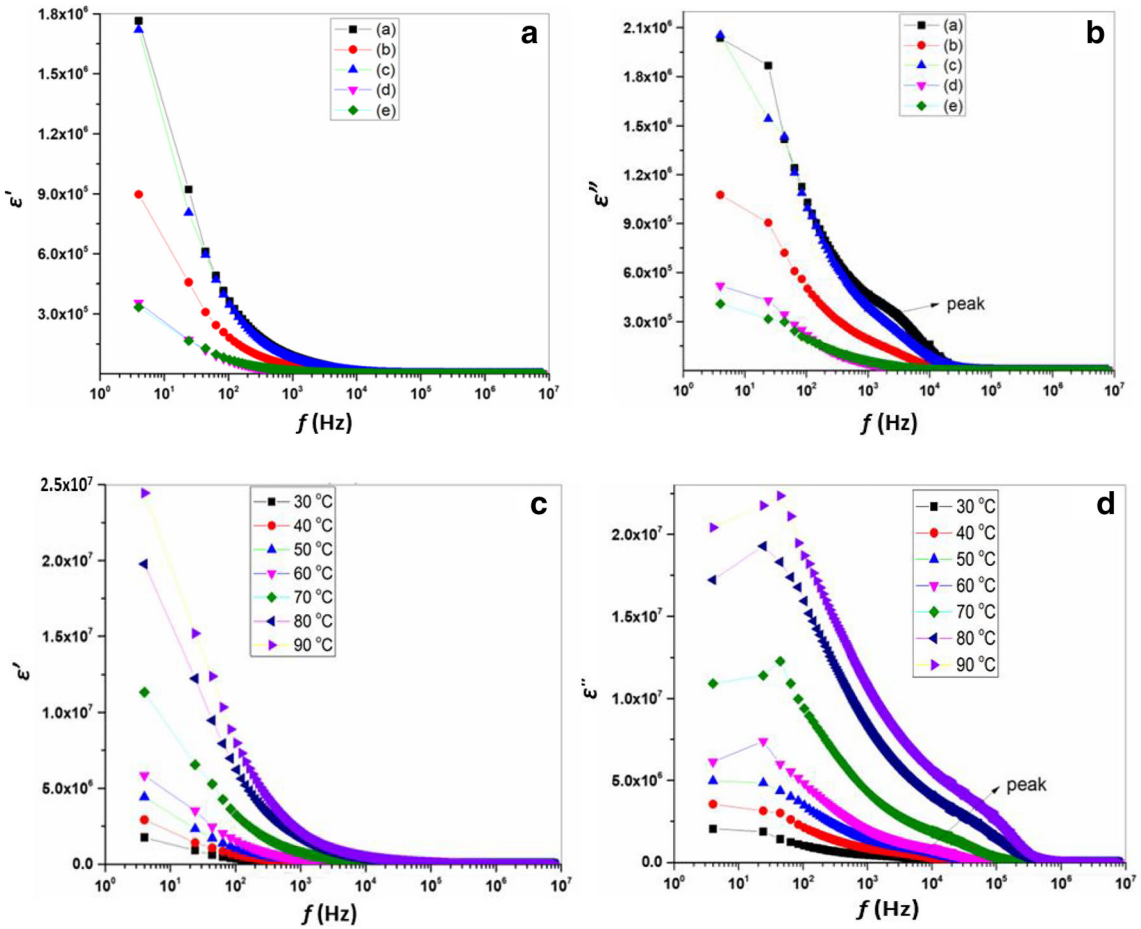

Fig. 9 Frequency-dependent dielectric permittivity spectra (ε' and ε'' vs. frequency) for **a**, **b** *BPBE-1* to *BPBE-5* at 30 °C and **c**, **d** for sample *BPBE-1* at different temperatures

electrolyte interface as a result of electrode polarization [31, 32]. But, at high frequency, inability of dipole orientation/chain relaxation due to the fast reversal of electric field results in a constant values of ε' and ε'' [21]. Further, in the case of crystalline and semi-crystalline polymeric materials, the crystalline phase dissolves effectively into amorphous phase with increase in temperature.

Temperature and concentration dependence dielectric permittivity study

The dielectric permittivity (ε' and ε'') values as a function of CS content (10–50 in wt%) at 30 °C and also as a function of temperature (30–100 °C) for sample *BPBE-1* at different fixed frequencies (4 Hz to 8 MHz) are plotted in Fig. 10a–d, respectively. The concentration-dependent ε' and ε'' study reveals that both these values vary irregularly (optimum for *BPBE-1*) and decrease with increasing frequency (Fig. 10a, b). The sample *BPBE-1* has the optimum dielectric permittivity values that indicates the availability of large number of free charge carriers near the electrode–electrolyte interface at room temperature and hence optimum σ_{dc}, N, and μ ($\sigma_{dc} = Nq\mu$). From Fig. 10c, d, it is observed that both the values of ε' and ε'' increase with increasing temperature and decreased with frequency. This is possibly due to re-orientation of dipoles associated with functional groups of polymer-biopolymer chains [21, 23]. The dielectric permittivity study of BPBE-1 film in the temperature range 30–100 °C shows that its dielectric characteristics are thermally activated.

Loss tangent (tanδ) study

The study of loss tangent (tanδ) spectra provides more insight about polymer chain relaxation. Figure 11 shows the variation of tanδ ($= \frac{\varepsilon''}{\varepsilon'} = \frac{M''}{M'}$) with frequency for (a) *BPBE-1* to *BPBE-5* at 30 °C and (b) for *BPBE-1* at different temperatures. The values of relaxation time,τ_r, were estimated from Fig. 11a by using the relation $\tau_r\omega_{peak} = 1$ where τ_r is the relaxation time in second and $\omega_{peak}(=2\pi f_{peak})$ is the maximum value of angular frequency of the applied signal. From Fig. 11a, it is observed that the $\tan\delta_{peak}$ shifted/changes by varying the CS

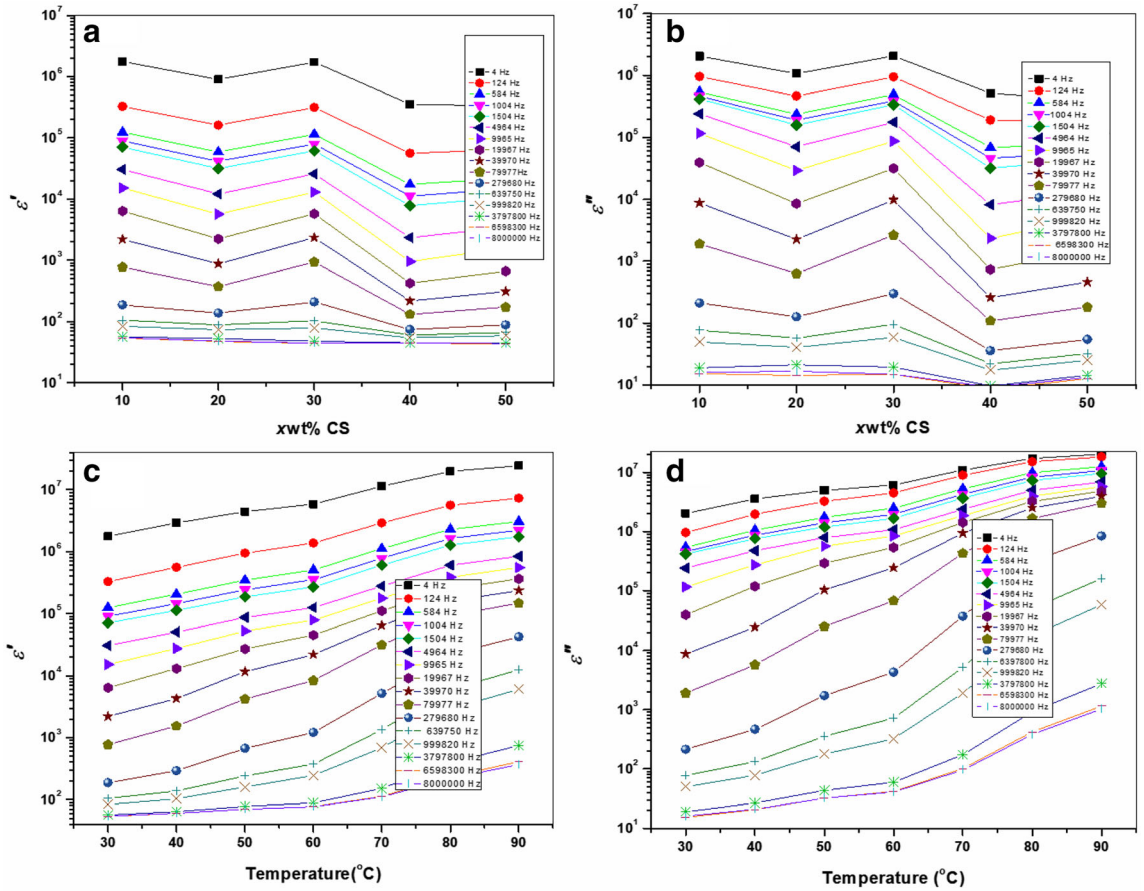

Fig. 10 **a**, **b** CS concentration-dependent plots of ε′ and ε″ for prepared *BPBE* films at 30 °C and **c**, **d** temperature-dependent plots of ε′ and ε″ for *BPBE-1* at selected frequencies

concentration in BPBE films due to change/modification in polymer chain relaxation and *BPBE-1* has the maximum relaxation frequency (τ_r is minimum). The tanδ increases with frequency, achieved a maxima, and then decreases and the value of tanδ shifted towards higher frequency side with increasing temperature due to increment in number of charge carriers in the electrolyte. Figure 12 a shows the variation of τ_r with temperature for sample *BPBE-1* to *BPBE-5* at different temperatures. The values of τ_r were found to change significantly up to 60 °C while at higher temperature (above 60 °C), its values are almost the same due to higher flexibility (polymer chain relaxation becomes faster at higher temperature). The relaxation frequency, f_r, shifted towards higher frequency side with increasing temperature for *BPBE-1*-based film (Fig. 11b). All other samples also show the same behavior as observed for sample *BPBE-1*. The motion of charge carriers becomes easier with increasing temperature and moving ions follow the change in direction of the field and relaxed even at higher frequency [33]. Hence, the peak observed in tanδ vs frequency curves shifted towards higher frequency side with increasing temperature.

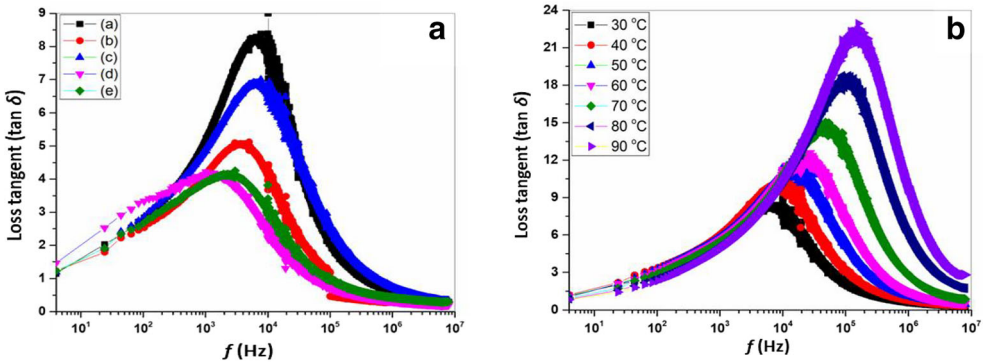

Fig. 11 Variation of loss tangent, tanδ with frequency for **a** *BPBE-1* to *BPBE-5* with different composition of CS at 30 °C and **b** *BPBE-1* at different temperatures

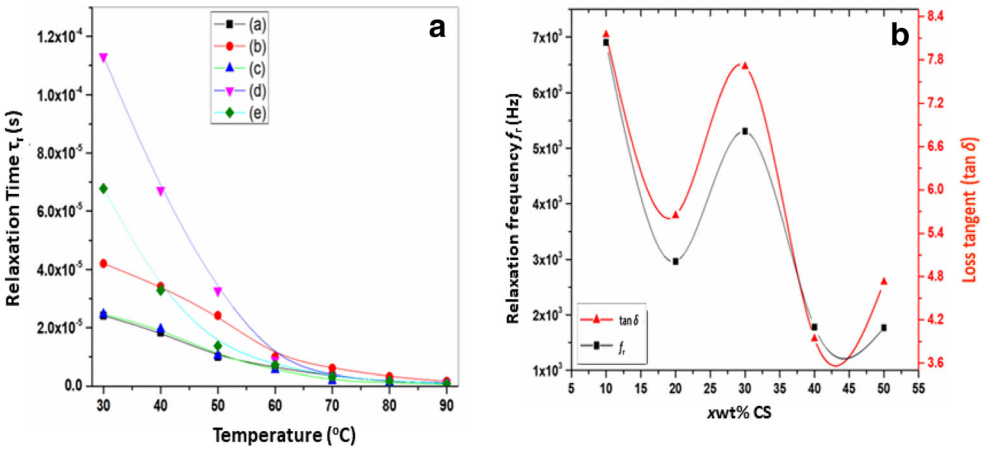

Fig. 12 **a** Relaxation time vs. temperature plot for samples *BPBE-1* to *BPBE-5* having different CS content and **b** relaxation frequency, loss tangent vs. concentration of CS plot at 30 °C

Scaling of loss tangent spectra (tanδ)

The scaling of tanδ spectra provides more insight about the variation of relaxation time with the applied electric field and can be described by the empirical Kohlrausch-Williams-Watt's law [34] expressed as

$$\psi(t) = \exp\left(\frac{-t}{\tau_r}\right)^{\beta} \tag{7}$$

where $\tau_r (= 1/2\pi f_{peak})$ is the relaxation time and β is the Kohlrausch exponent $(=\frac{1.44}{FWHM})$. For Debye type relaxation behavior, the value of $\beta = 1$ and full width at half maximum (FWHM) for typical Debye peak = 1.44 [35]. Generally, for polymer electrolytes, many researchers reported the value of $\beta < 1$ [36]. In this work, the scaling of tanδ spectra were performed with respect to CS content and temperatures are shown in Fig. 13 a and b, respectively. From Fig. 13a, it has been observed that all the spectra collapse into single master curve except in low frequency region while scaling with respect to temperature, spectra collapse into a single curve (Fig. 13b). The full width at half maxima (FWHM) of tanδ vs frequency plots for *BPBE-1* to *BPBE-5* at 30 °C (Fig. 13a and for *BPBE-1* at different temperatures (Fig. 13b) have been estimated and found that its values lie in the range 0.24 to 0.15 and 0.24–0.25, respectively. The value of β is quite low for studied samples which shows that present system has non-Debye type relaxation mechanism.

Electric modulus study

The complex dielectric modulus spectra are used very frequently to understand the conductivity relaxation. Present BPBE film has different functional groups like hydroxyl (O–H) group associated with CS and PVA, amine (NH_2), and amide (C=O–NHR) associated with CS. Therefore, in dielectric relaxation process, the re-orientation of polar groups with side chains of polymer may be observed in electric modulus study. The real *(M′)* and imaginary (*M″*) parts of complex

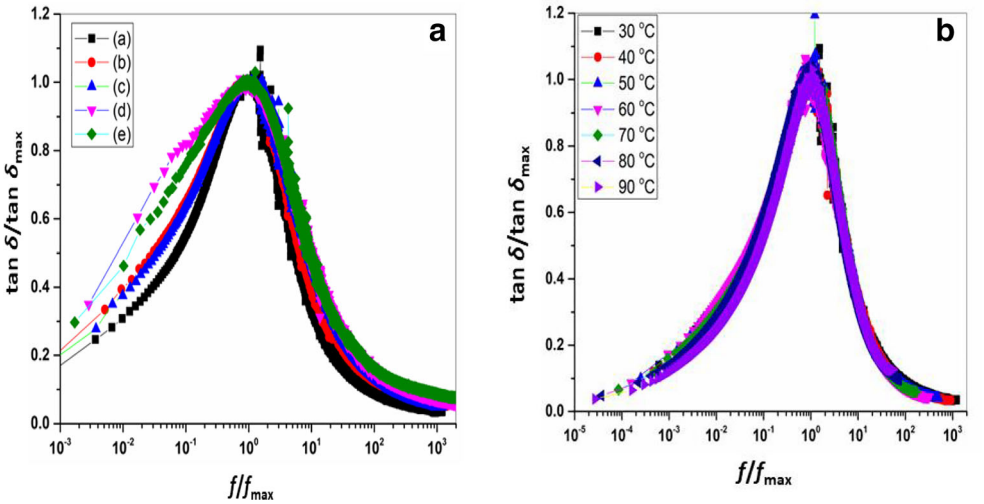

Fig. 13 Scaling of loss tangent spectra **a** at different CS concentration for prepared *BPBE* films at 30 °C and **b** at different temperatures for sample *BPBE-1*

electric modulus (M^*) (i.e., reciprocal of complex dielectric permittivity ($\varepsilon^*(f)$) can be calculated by using the impedance spectroscopic data, expressed as

$$M^* = \frac{1}{\varepsilon^*(f)} = M' + jM'' \tag{8}$$

The variation M' and M'' with frequency for *BPBE-1* to *BPBE-5* at 30 °C and for *BPBE-1* at different temperatures are shown in Fig. 14 a, b and c, d, respectively. The M' spectra has long tail at low frequency for CS-dependent films as well as for *BPBE-1* at different temperature and then the value of M' increases exponentially with frequency and a small peak were observed which were found to shifts towards higher frequency side with increasing temperature (Fig. 14 a and c). The presence of long tail at low frequency is because of large capacitive effect (ε' is high in low frequency region) associated with electrode polarization [15, 23]. The M'' spectra for *BPBE-1* to *BPBE-5* at 30 °C (Fig. 14b) and for *BPBE-1* at different temperatures (Fig. 14d) have the distinct relaxation peaks and these peaks were shifted with CS concentration as well as by changing the temperature related to the conductivity relaxation and strong coupling between the free ions and segmental motion of polymer chains [37].

Ionic transference number measurement

ITN is very essential feature of an electrolyte that gives the information about the nature of charge carrier species that is an ionic or electronic. The ITN measurement has been performed using Keithley-2450 source meter. The Wegner's dc polarization technique was used for the determination of ITN [21]. In this measurement, two-electrode method was used with constant low dc voltage on the cell assembly *SS* | *BPBEs* | *SS*. Figure 15 shows a typical current vs. time plot for BPBE-1 at 30 °C. Similar current vs. time plots were observed for all other sample and the values of ionic ITN are listed in Table 4. The ITN, T_{ion} was calculated from the polarization curve (Fig. 15) by using the expression:

$$T_{ion} = \frac{I_t - I_e}{I_t} \tag{9}$$

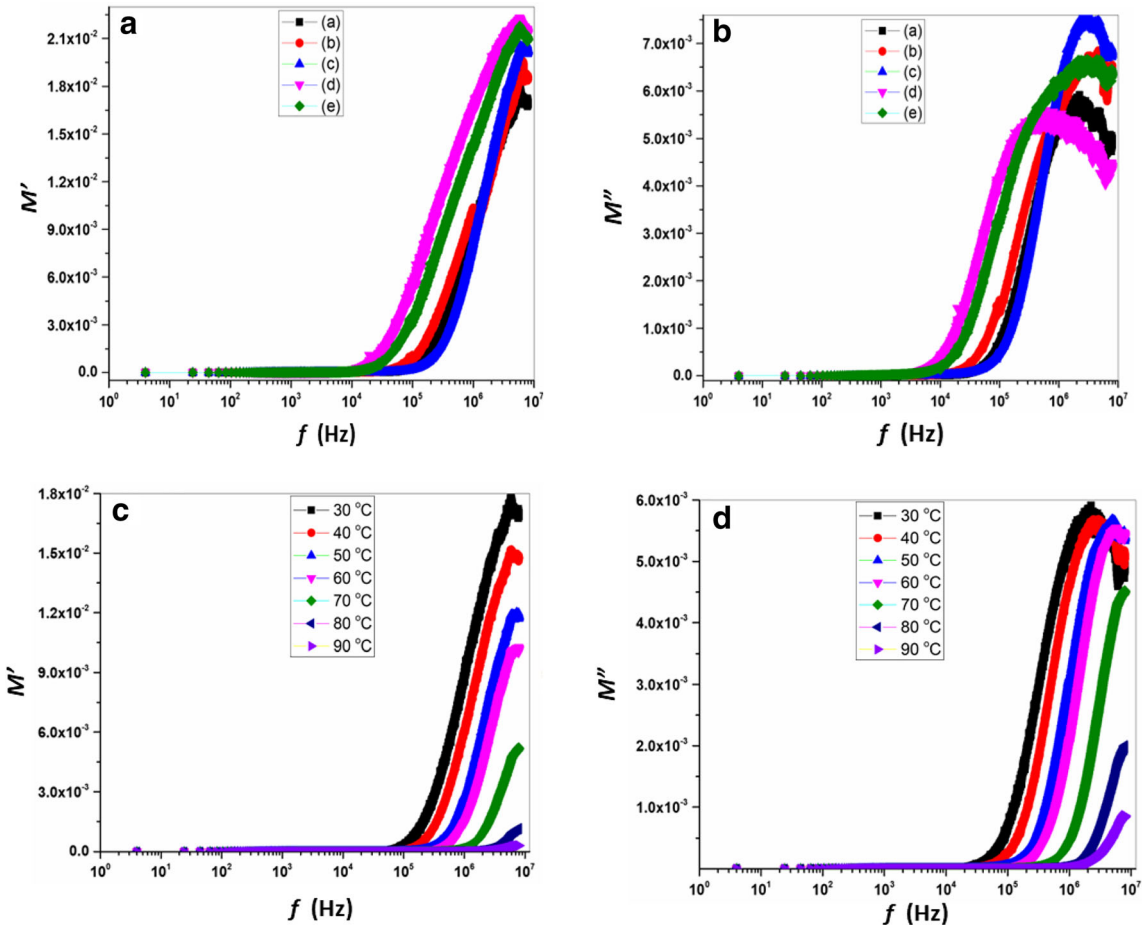

Fig. 14 Variation of electric modulus as a function of frequency for **a** BPBE-1 to BPBE-5 samples with different composition of CS at 30 °C and **b** sample *BPBE-1* at different temperatures

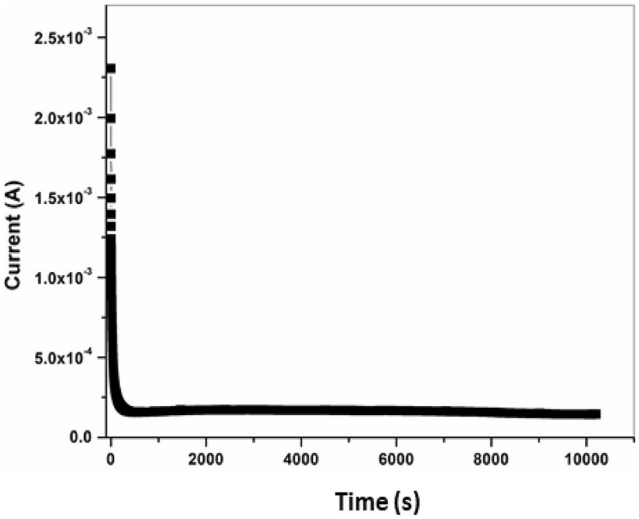

Fig. 15 Polarization current vs. time plot for sample *BPBE-1* at 30 °C

where I_t is the sum of ionic and electronic currents (total current) and I_e is the electronic current (residual current). The ITN was found to be nearly 0.94–0.98 for studied BPBE films. These values of ITN strongly suggest that the charge transport in these BPBEs is predominately due to ions only.

CV measurement

To study the electrochemical stability (ES) of the prepared BPBE film, a cyclic voltammetry (CV) measurement has been performed using power source meter Keithley-2450 at the scan rate 25 mV s^{-1} for 8 cycles using solid state method. ES for an electrolyte is very useful parameter which determines the maximum potential limit applied on the electrolyte for device applications point of view [38]. The optimized sample, *BPBE-1*, was sandwiched in between stainless steel electrodes, i.e., *SS*|*BPBE-1*|*SS* cell assembly for CV measurement. For taking the CV data, cyclic sweeping in the voltage range − 2 to + 2 V has been done and current vs. voltage plot for sample *BPBE-1* is shown in Fig. 16. The CV plot has symmetry oxidation and reduction peaks which confirm the good electro-chemical behavior of optimized sample, BPBE-1. The peaks observed in closed CV curves reveal the intercalation/de-intercalation phenomenon or Faradaic process near the electrode-electrolyte interface [39, 40].

Conclusions

BPBE films, i.e., *BPBE-1* to *BPBE-5*, were prepared by using solution casting method and optimized. The sample *BPBE-1* shows the optimum ionic conductivity ~ 1.2×10^{-5} S cm^{-1} with maximum N and μ values at 30 °C. IR spectroscopic results show the interactions/complexation between the functional groups of CS-PVA with Na^+/I^- of the dissociated salt, NaI. XRD analysis reveals the amorphousness of the prepared BPBE samples having single characteristic peak that appeared at $2\theta \sim 23°$. TGA supported by 1st DTGA analysis shows that films are decomposed in multi-steps and it is also evident in the complexation that occurred in between CS-PVA/NaI. AC conductivity spectrum of BPBE films at different CS concentration as well as at different temperatures for *BPBE-1* follows the JPL with $n < 1$. Log σ vs. $1/T$ and log f_r vs. $1/T$ plots for BPBE films follows the Arrhenius type behavior. The scaling of tanδ with CS concentrations/temperatures shows that BPBE has non-Debye type relaxation mechanism. The $\tan\delta_{peak}$ shifted/changes by varying the CS concentration in BPBE films due to change/modification in polymer chains relaxation and *BPBE-1* has the maximum relaxation frequency (τ_r is minimum). Electrode polarization, conductivity relaxation, and strong coupling between the free ions and segmental motion of polymer chains were

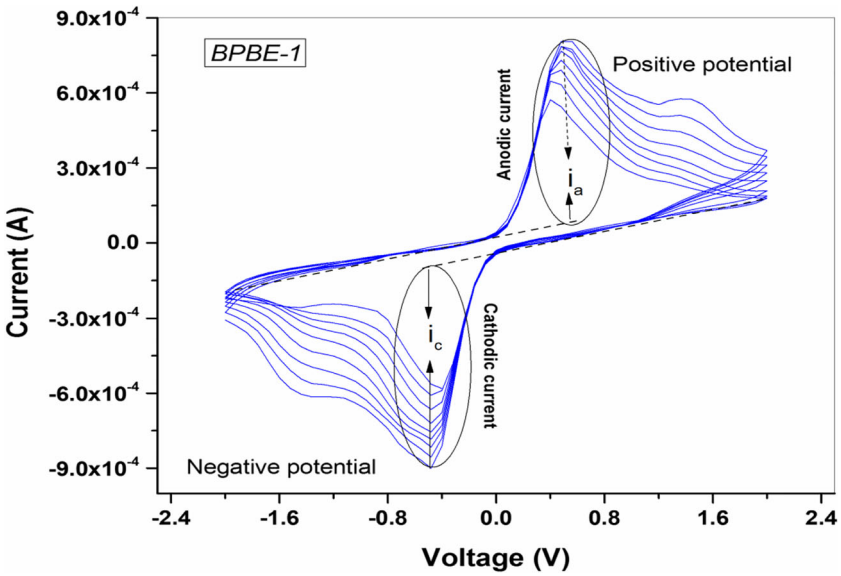

Fig. 16 Cyclic voltammogram of sample, *BPBE-1* at the scan rate 25 mV s^{-1}

observed in dielectric permittivity and electric modulus studies. The ITN was found to be nearly 0.94–0.98 that suggests that the charge transportation in these BPBEs is predominately due to ions only. The symmetry oxidation and reduction peaks in CV plot confirm the good electro-chemical behavior of optimized sample, *BPBE-1*.

Funding One of the authors, ALS, received financial assistance from SERB, India, through research project EEQ/2018/000862.

References

1. Varshney PK, Gupta S (2011) Natural polymer-based electrolytes for electrochemical devices: a review. Ionics 17(6):479–483
2. Gaikwad UV, Pande SA (2013) A review of biopolymer chitosan blends in polymer system. Int Res J Sci Eng 1(1):13–16
3. Kadir MFZ, Majid SR, Arof AK (2010) Plasticized chitosan-PVA blend polymer electrolyte based proton battery. Electrochim Acta 55(4):1475–1482
4. Dutta PK, Dutta J, Tripathi VS (2004) Chitin and chitosan: chemistry, properties and applications. J Sci Ind Res 63:20–31
5. Aziz SB, Abdullah OG, Rasheed MA, Ahmed HM (2017) Effect of high salt concentration (HSC) on structural, morphological, and electrical characteristics of chitosan based solid polymer electrolytes. Polymers 9(12):187
6. Leones R, Sabadini RC, Esperança JMSS, Pawlicka A, Silva MM (2017) Effect of storage time on the ionic conductivity of chitosan-solid polymer electrolytes incorporating cyano-based ionic liquids. Electrochim Acta 232:22–29
7. Jaafar NK, Lepit A, Aini NA, Ali AMM, Saat A, Yahya MZA (2014) Structural and electrical properties of plasticized radiation induced chitosan grafted poly(methyl methacrylate) polymer electrolytes. Int J Electrochem Sci 9(2):821–829
8. Vijaya N, Selvasekarapandian S, Sornalatha M, Sujithra KS, Monisha S (2017) Proton-conducting biopolymer electrolytes based on pectin doped with NH4X (X=Cl, Br). Ionics 23(10): 2799–2808
9. Puteh R, Yahya MZA, Ali AMM, Sulaiman M, Yahya R (2005) Conductivity studies on chitosan-based polymer electrolytes with lithium salts. Indonesian J Phys 16:17–19
10. Van Soest JJG, Knooren N (1997) Influence of glycerol and water content on the structure and properties of extruded starch plastic sheets during aging. J Appl Polym Sci 64(7):1411–1422
11. Khiar ASA, Puteh R, Arof AK (2006) Conductivity studies of a chitosan-based polymer electrolyte. Phys B Condens Matter 373(1):23–27
12. Navaratnam S, Ramesh K, Ramesh S, Sanusi A, Basirun WJ, Arof AK (2015) Transport mechanism studies of chitosan electrolyte systems. Electrochim Acta 175:68–73
13. Abutalib MM, Rajeh A (2020) Structural, thermal, optical and conductivity studies of Co/ZnO nanoparticles doped CMC polymer for solid state battery applications. Polym Test 91:106803
14. Agrawal P, Strijkers GJ, Nicolay K (2010) Chitosan-based systems for molecular imaging. Adv Drug Deliv Rev 62(1):42–58
15. Saroj AL, Singh RK (2012) Thermal, dielectric and conductivity studies on PVA/Ionic liquid [EMIM][EtSO4] based polymer electrolytes. J Phys Chem Solids 73(2):162–168
16. Saroj AL, Krishnamoorthi S, Singh RK (2017) Structural, thermal and electrical transport behaviour of polymer electrolytes based on PVA and imidazolium based ionic liquid. J Non-Cryst Solids 473: 87–95
17. Mobarak NN, Ahmad A, Abdullah MP, Ramli N, Rahman MYA (2013) Conductivity enhancement via chemical modification of chitosan based green polymer electrolyte. Electrochim Acta 92: 161–167
18. Kadir MFZA, Abdul MFZ, Teo LP, Majid SR, Arof AK (2009) Conductivity studies on plasticized PEO/chitosan proton conducting polymer electrolyte. Mater Res Innov 13(3):259–262
19. Kadir MFZ, Aspanut Z, Majid SR, Arof AK (2011) FTIR studies of plasticized poly(vinyl alcohol)-chitosan blend doped with NH4NO3 polymer electrolyte membrane. Spectrochim Acta A 78(3):1068–1074
20. Hezma AM, Rajeh A, Mohammed AM (2019) An insight into the effect of zinc oxide nanoparticles on the structural, thermal, mechanical properties and antimicrobial activity of Cs/PVA composite. Colloids and Surfaces A: Physicochem Eng Aspects 581: 123821
21. Bharati DC, Kumar H, Saroj AL (2019) Chitosan-PEG-NaI based bio-polymer electrolytes: structural, thermal and ion dynamics studies. Mater Res Express 6:125360
22. Ragab HM, Rajeh A (2020) Structural, thermal, optical and conductive properties of PAM/PVA polymer composite doped with Ag nanoparticles for electrochemical application. J of Mat Science: Materials in Electronics 31:16780–16792
23. Singh P, Bharati DC, Gupta PN, Saroj AL (2018) Vibrational, thermal and ion transport properties of PVA-PVP-PEG-$MeSO_4Na$ based polymer blend electrolyte films. J Non-Cryst Solids 494:21–30
24. Sudhakar YN, Selvakumar M (2012) Lithium perchlorate doped plasticized chitosan and starch blend as biodegradable polymer electrolyte for supercapacitors. Electrochim Acta 78:398–405
25. Aziz SB, Woo TJ, Kadir MFZ, Ahmed HM (2018) A conceptual review on polymer electrolytes and ion transport models. Journal of Science: Advanced Materials and Devices 3(1):1–17
26. Perumal P, Christopher Selvin P, Selvasekarapandian S, Sivaraj P, Abhilash KP, Moniha V, Manjula Devi R (2019) Plasticizer incorporated, novel eco-friendly bio-polymer based solid bio-membrane for electrochemical clean energy applications. Polym Degrad Stab 159:43–53
27. Jonscher AK (1977) The 'universal' dielectric response. Nature 267(5613):673–679
28. Sohaimy MIH, Isa MIN (2017) Ionic conductivity and conduction mechanism studies on cellulose based solid polymer electrolytes doped with ammonium carbonate. Polym Bull 74(4):1371–1386
29. Arya A, Sharma AL (2018) Optimization of salt concentration and explanation of two peak percolation in blend solid polymer nanocomposite films. J Solid State Electrochem 22(9):2725–2745
30. Aziz SB (2013) Li+ ion conduction mechanism in poly (ε-caprolactone)-based polymer electrolyte. Iran Polym J 22(12): 877–883
31. Saroj AL, Singh RK, Chandra S (2013) Studies on polymer electrolyte poly(vinyl) pyrrolidone (PVP) complexed with ionic liquid: Effect of complexation on thermal stability, conductivity and relaxation behaviour. Mater Sci Eng B 178(4):231–238
32. Sudhakar YN, Selvakumar M, Bhat DK (2014) Tubular array, dielectric, conductivity and electrochemical properties of biodegradable gel polymer electrolyte Mater. Sci Eng B180(1):12–19
33. Kumar S, Prajapati GK, Saroj AL, Gupta PN (2019) Structural, electrical and dielectric studies of nano-composite polymer blend electrolyte films based on (70–x) PVA–x PVP–NaI–SiO_2. Phys B Condens Matter 554:158–164
34. Williams G, Watts DC (1970) Non-symmetrical dielectric relaxation behavior arising from a simple empirical decay function. Trans Faraday Soc 66:80–85
35. Patel HK, Martin SW (1992) Fast ionic conduction in $Na_2S+B_2S_3$ glasses: compositional contributions to nonexponentiality in

conductivity relaxation in the extreme low-alkali-metal limit. Phys Rev B 45(18):10292–10300
36. Dieterich W, Maass P (2002) Non-Debye relaxations in disordered ionic solids. Chem Phys 284(1-2):439–467
37. Das S, Ghosh A (2015) Effect of plasticizers on ionic conductivity and dielectric relaxation of PEO-LiClO4 polymer electrolyte. Electrochim Acta 171:59–65
38. Kadir MFZ, Salleh NS, Hamsan MH, Aspanut Z, Majid NA, Shukur MF (2018) Biopolymeric electrolyte based on glycerolized methyl cellulose with NH4Br as proton source and potential application in EDLC. Ionics 24(6):1651–1662
39. Rasali NMJ, Saadiah MA, Zainuddin NK, Nagao Y, Samsudin AS (2020) Ionic transport studies of solid bio-polymer electrolytes based on carboxymethyl cellulose doped with ammonium acetate and its potential application as an electrical double layer capacitor. Express Polym Lett 14(7):619–637
40. Agrawal SL, Shukla PK, Tripathi D, Singh CP (2019) Studies on multiferroic oxide-doped PVA-based nanocomposite gel polymer electrolyte system for electrochemical device application. Ionics 25(2):617–626